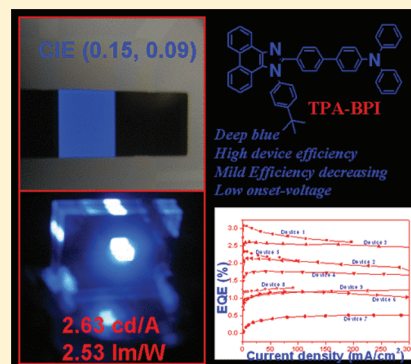


High Efficiency Nondoped Deep-Blue Organic Light Emitting Devices Based on Imidazole- $\pi$ -triphenylamine DerivativesYing Zhang,<sup>†,‡</sup> Shiu-Lun Lai,<sup>‡</sup> Qing-Xiao Tong,<sup>†,§,\*</sup> Ming-Fai Lo,<sup>‡</sup> Tsz-Wai Ng,<sup>‡</sup> Mei-Yee Chan,<sup>||</sup> Zhi-Chun Wen,<sup>†</sup> Jun He,<sup>⊥</sup> Kc-Sham Jeff,<sup>⊥</sup> Xiang-Lin Tang,<sup>#</sup> Wei-Min Liu,<sup>#</sup> Chi-Chiu Ko,<sup>⊥</sup> Peng-Fei Wang,<sup>#</sup> and Chun-Sing Lee<sup>‡,\*,\*</sup><sup>†</sup>Department of Chemistry, Shantou University, Guangdong 515063, China<sup>‡</sup>Center of Super-Diamond and Advanced Films (COSDAF) and Department of Physics and Materials Science and <sup>⊥</sup>Department of Biology and Chemistry, City University of Hong Kong, Hong Kong SAR, China<sup>§</sup>Jiangsu Key Laboratory for Carbon-Based Functional Materials & Devices, Soochow University, China<sup>||</sup>Department of Chemistry, The University of Hong Kong, Hong Kong SAR, China<sup>#</sup>Technical Institute of Physics and Chemistry, Chinese Academy of Sciences, Beijing 100190, China

## S Supporting Information

**ABSTRACT:** High-performance deep-blue emitting phenanthroimidazole derivatives with a structure of donor–linker–acceptor were designed and synthesized. By using different linkers and different linking positions, four deep-blue emitters were obtained and used as emitters or bifunctional hole-transporting emitters in OLEDs. Such devices show low turn-on voltages (as low as 2.8 V), high efficiency (2.63 cd/A, 2.53 lm/W, 3.08%), little efficiency roll-off at high current densities, and stable deep-blue emissions with CIE<sub>y</sub> < 0.10. Performances are among the best comparing to recently reported deep-blue emitting devices with similar structures. The results suggest that the combination of the phenanthroimidazole and the donor–linker–acceptor structure can be an important approach for developing high performance deep-blue emitters in particular for lighting applications.

**KEYWORDS:** high efficiency, nondoped, deep-blue organic light emitting devices



## ■ INTRODUCTION

Blue organic light-emitting devices (OLEDs) have attracted much attention for their importance in both full-color display and solid-state lighting.<sup>1</sup> Given that phosphorescent OLEDs can theoretically achieve 100% internal quantum efficiency, many researchers have reported phosphorescent materials with high efficiency deep-blue emission.<sup>2</sup> However, phosphorescence OLEDs typically have shorter lifetime and sharper efficiency roll-off at high brightness. Thus, phosphorescence and fluorescence OLEDs are often considered to be complementary and suitable for different applications. On the other hand, many high performance OLEDs involve doping of emitters into host materials.<sup>3</sup> However, efficacious doping often requires precise control of doping concentration and inevitably increases manufacturing cost. It has also been pointed out that potential phase separation in the dopant–host system can render energy transfer ineffective.<sup>4</sup> For these reasons, nondoped devices using blue light-emitting fluorescent OLEDs are still attracting considerable attention.

While many high efficiency blue fluorescent materials have been reported, many of them give sky-blue emissions instead of saturated blue with CIE<sub>y</sub> < 0.10.<sup>5</sup> On the other hand, many saturated blue emitters were designed with incorporation of the

electron-withdrawing moiety for easier electron injection. However, these materials typically also have deep highest occupied molecular orbital (HOMO) leading to larger hole–injection barriers at the hole-transporter/emitter junctions and thus higher operation voltages as well as lower efficiencies.<sup>6,8–18</sup> In fact, deep-blue OLEDs with high efficiency, good color stability, and low onset/working voltage are rare.

Charge transport and balancing are key factors for obtaining high device efficiency. Recently some deep-blue emitters were realized by simultaneously incorporating donor and acceptor groups into one molecule and proved to be a promising method for obtaining a high performance deep-blue emitter.<sup>7,20–23</sup> In this work, we use the donor– $\pi$ -acceptor approach to design three new molecules by using phenanthroimidazole as the acceptor for its good electron-transporting mobility and triphenylamine (TPA) as the donor for its good hole transport mobility and connecting them with different linkers (benzene or thiophene); TPA-TPI was used here for comparison. By attaching TPA to different position (1- or 2-) of the imidazole

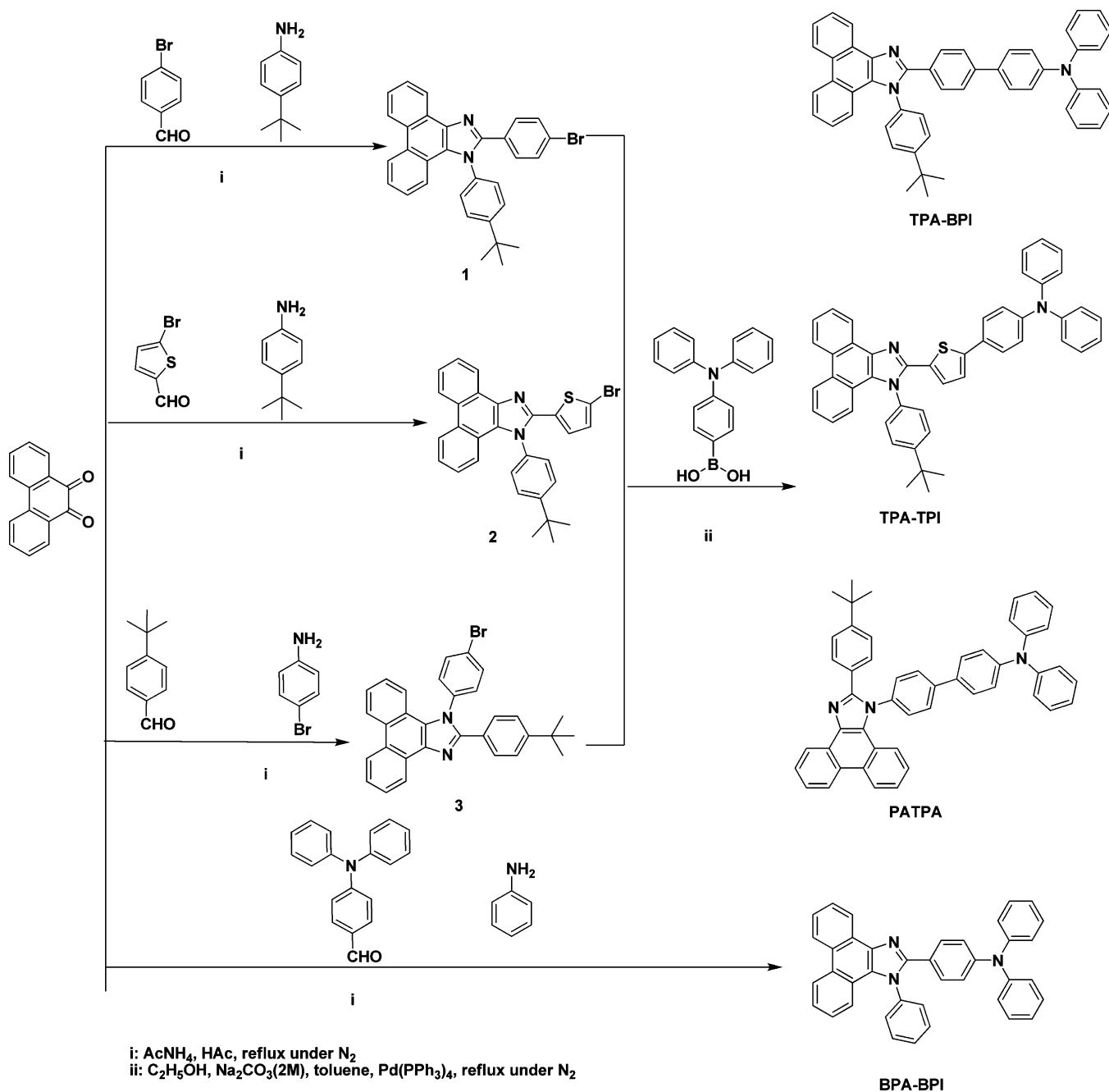
Received: June 23, 2011

Revised: November 29, 2011

Published: November 29, 2011



Scheme 1. Synthetic Routes for the TPA–Imidazole Derivatives



ring (acceptor) with different linkers, we investigated their differences in photophysical properties and effects on orbital energy levels. The new emitters were found to give deep-blue emissions with fluorescent quantum yield as high as unity. In addition, the compounds also have good hole-transporting properties. OLEDs using these emitters were observed to deliver high efficiencies of 2.63 cd/A and 2.53 lm/W at deep-blue color with CIE<sub>y</sub> coordinate smaller than 0.10. In addition to low turn-on (e.g., 2.8 V) and operation voltages, the present devices also show stable emission colors and little efficiency roll-off at high brightness output. In terms of these performance parameters, some of the new compounds described here are among the best nondoped deep-blue emitters reported recently.

## EXPERIMENT AND CHARACTERIZATION

All solvents and materials were used as received from commercial suppliers without further purification. Synthetic routes of the four compounds are outlined in Scheme 1. 2-(4-Bromophenyl)-1-(4-*tert*-butylphenyl)-1*H*-phenanthro[9,10-*d*]imidazole (1), 2-(5-bromothiophen-2-yl)-1-(4-*tert*-butyl phenyl)-1*H*-phenanthro[9,10-*d*]imidazole (2), 1-(4-bromophenyl)-2-(4-*tert*-butylphenyl)-1*H*-phenanthro[9,10-*d*]imidazole (3), and BPA-BPI were prepared according to the literature.<sup>24</sup> Compounds TPA-BPI, TPA-TPI, and PATPA were prepared through Suzuki coupling reactions.<sup>25</sup> Other than the three new compounds, a reported imidazole- $\pi$ -triphenylamine derivative TPA-TPI was also used here for comparison.<sup>27</sup>

Nuclear magnetic resonance (NMR) spectra were recorded using  $\text{CD}_2\text{Cl}_2$  as solvent with a Varian Gemin-400 or Varian Gemin-300 spectrometer. Mass spectra were recorded on a PE SCIEX API-MS spectrometer. Single crystal structures of TPA-BPI and BPA-BPI were

further studied by X-ray diffraction with a Gemini A Ultra X-ray single crystal diffractometer using graphite monochromatized Mo K $\alpha$  radiation (Mo K $\alpha$ ,  $\lambda = 0.71073$  Å). The crystallographic calculations were conducted using the SHELXL-97 program. Absorption and photoluminescence (PL) spectra of the materials were recorded on a Perkin-Elmer Lambda 2S UV–visible spectrophotometer and Perkin-Elmer LS50 fluorescence spectrometer, respectively. Fluorescence quantum yields ( $\Phi_f$ ) in dichloromethane solution were determined according to the previous literature<sup>26</sup> by a comparative method, using anthracene as a standard reference with  $\Phi_f = 0.27$  in ethanol. Thermogravimetric (TGA) measurements were performed on a TA Instrument TGAQ50 at a heating rate of 10 °C/min under a nitrogen environment. Differential scanning calorimetric (DSC) measurements were performed on a TA Instrument DSC2910. The samples were first heated at a rate of 10 °C/min to melt and then quenched. The glass transition temperature ( $T_g$ ) and crystallization temperature ( $T_c$ ) were recorded by heating the quenched samples at a heating rate of 10 °C/min. Ionization potential ( $I_p$ ) of the materials were measured on ITO glass substrates in a thin-film state via ultraviolet photoelectron spectroscopy (UPS) in a VG ESCALAB 220i-XL surface analysis system, while the values of electron affinity ( $E_A$ ) were estimated by subtracting from  $I_p$  with the optical band gap ( $E_{gap}$ ) determined from the absorption spectra of their solid-state films. Theoretical calculations of the distributions of HOMO and lowest unoccupied molecular orbital (LUMO) were performed with the method of B3LYP/6-31G (d).

## SYNTHESIS

**2-(4-Bromophenyl)-1-(4-*tert*-butylphenyl)-1*H*-phenanthro[9,10-*d*]imidazole (1).** The product was prepared by refluxing 9,10-phenanthrenequinone (2.12 g, 10 mmol), 4-bromobenzaldehyde (1.86 g, 10 mmol), 4-*tert*-butylbenzenamine (1.92 mL, 12 mmol), and ammonium acetate (9.49 g, 122.3 mmol) in glacial acetic acid (50 mL) for 24 h under an argon atmosphere. After cooling to room temperature, a pale yellow mixture was obtained and poured into a methanol solution under stirring. The separated solid was filtered off, washed with methanol, and dried to give a pale yellow solid. The solid was purified by column chromatography (petroleum ether: CH<sub>2</sub>Cl<sub>2</sub>, 1:1) on silica gel. A white powder was finally obtained after it was stirred in refluxing ethanol, subsequently filtered, and dried in vacuum. Yield: 4.03 g (79%). <sup>1</sup>H NMR (300 MHz; CD<sub>2</sub>Cl<sub>2</sub>; Me<sub>4</sub>Si)  $\delta_H$  [ppm]: 1.47 (s, 9H), 7.16–7.83 (m, 13H), 8.76 (dd,  $J = 15.2, 8.2$  Hz, 3H).  $\delta_C$  (75 MHz; CD<sub>2</sub>Cl<sub>2</sub>; Me<sub>4</sub>Si) 31.32 (s), 35.15 (s), 121.18 (s), 122.62 (s), 123.30 (d), 124.20 (s), 125.16 (s), 125.77 (s), 126.53 (s), 127.46 (d), 128.49 (d), 129.33 (s), 130.05 (s), 130.91 (s), 131.47 (s), 135.98 (s), 137.46 (s), 149.88 (s), 153.90 (s). MS (ESI<sup>+</sup>):  $m/z$  505.5 (MH<sup>+</sup>). Calcd for C<sub>31</sub>H<sub>23</sub>BrN<sub>2</sub>: 504.12.

**2-(5-Bromothiophen-2-yl)-1-(4-*tert*-butylphenyl)-1*H*-phenanthro[9,10-*d*]imidazole (2).** The synthesis procedure is according to our previous work.<sup>27</sup> Yield: 8 g (78%). <sup>1</sup>H NMR (400 MHz; CD<sub>2</sub>Cl<sub>2</sub>; Me<sub>4</sub>Si)  $\delta_H$  [ppm]: 1.52 (s, 9H), 6.50 (d,  $J = 4$  Hz, 1H), 6.89 (d,  $J = 4$  Hz, 1H), 7.20 (dd,  $J = 8.3, 0.8$  Hz, 1H), 7.25–7.34 (m, 1H), 7.49–7.59 (m, 3H), 7.64–7.81 (m, 4H), 8.70–8.81 (m, 3H). MS (ESI<sup>+</sup>):  $m/z$  511.4 (MH<sup>+</sup>). Calcd for C<sub>29</sub>H<sub>23</sub>BrN<sub>2</sub>S: 510.08.

**1-(4-Bromophenyl)-2-(4-*tert*-butylphenyl)-1*H*-phenanthro[9,10-*d*]imidazole (3).** Using a similar approach for **1** by replacing 4-*tert*-butylbenzenamine and 4-bromobenzaldehyde with 4-bromobenzenamine and 4-*tert*-butylbenzaldehyde, a white powder was finally obtained. Yield: 5.08 g (67%). <sup>1</sup>H NMR (400 MHz; CD<sub>2</sub>Cl<sub>2</sub>; Me<sub>4</sub>Si)  $\delta_H$  [ppm]: 1.33 (s, 9H), 7.23 (d,  $J = 8.2$  Hz, 1H), 7.30–7.59 (m, 8H), 7.63–7.82 (m, 4H), 8.77 (dd,  $J = 17.3, 8.1$  Hz, 3H).  $\delta_C$  (75 MHz; CD<sub>2</sub>Cl<sub>2</sub>) 31.10 (s), 34.81 (s), 72.35 (s), 120.92 (s), 122.70 (s), 123.26 (d), 123.96 (s), 124.32 (s), 125.09 (s), 125.48 (s), 125.77 (s), 126.63 (s), 127.30–128.36 (m), 128.37 (s), 129.18 (d), 131.05 (s), 133.63 (s), 137.94 (d), 138.38–138.75 (m), 151.08 (s), 152.46 (s). MS (ESI<sup>+</sup>):  $m/z$  505.1 (MH<sup>+</sup>). Calcd for C<sub>31</sub>H<sub>23</sub>BrN<sub>2</sub>: 504.12.

***N*-Phenyl-*N*-(4-(1-phenyl-1*H*-phenanthro[9,10-*d*]imidazol-2-yl)phenyl)benzenamine (BPA-BPI).** Using a similar approach for **1** by replacing 4-*tert*-butylbenzenamine and 4-bromobenzaldehyde with aniline and 4-(diphenylamino)benzaldehyde, a light yellow powder

was finally obtained. Yield: 2.81 g (88%). mp: 272 °C. <sup>1</sup>H NMR (400 MHz; CD<sub>2</sub>Cl<sub>2</sub>; Me<sub>4</sub>Si)  $\delta_H$  [ppm]: 6.93 (d,  $J = 8.8$  Hz, 2H), 7.06–7.22 (m, 7H), 7.31 (t,  $J = 7.9$  Hz, 5H), 7.43–7.72 (m, 9H), 7.73–7.80 (m, 1H), 8.78 (dd,  $J = 21.5, 7.9$  Hz, 3H).  $\delta_C$  (75 MHz; CD<sub>2</sub>Cl<sub>2</sub>) 120.99 (s), 121.62 (s), 122.66 (s), 123.34 (s), 123.66–124.92 (m), 124.85 (s), 124.92–125.05 (m), 125.46 (d,  $J = 18.9$  Hz), 126.45 (s), 127.44 (d,  $J = 7.9$  Hz), 128.31 (s), 128.80–129.92 (m), 129.68–129.92 (s), 130.05 (d,  $J = 8.1$  Hz), 130.38 (s), 139.27 (s), 147.38 (s), 148.54 (s). MS (ESI<sup>+</sup>):  $m/z$  538.4 (MH<sup>+</sup>). Calcd for C<sub>39</sub>H<sub>27</sub>N<sub>3</sub>: 537.22.

***N*-(4-(4-(1-(4-*tert*-Butylphenyl)-1*H*-phenanthro[9,10-*d*]imidazol-2-yl)phenyl)phenyl)-*N*-phenylbenzenamine (TPA-BPI).** A solution of compound **1** (2.38 g, 4.7 mmol), 4-(diphenylamino)phenylboronic acid (1.74 g, 7.5 mmol), Pd(PPh<sub>3</sub>)<sub>4</sub> (0.29 g, 0.25 mmol), and aqueous Na<sub>2</sub>CO<sub>3</sub> (2 M, 18 mL) in toluene (36 mL) and ethanol (12 mL) was heated to reflux in an argon atmosphere for 24 h. The solution was cooled to room temperature and extracted with dichloromethane. The extracts were dried with anhydrous Na<sub>2</sub>SO<sub>4</sub> and concentrated by rotary evaporation. The residue was purified by column chromatography (petroleum ether: CH<sub>2</sub>Cl<sub>2</sub>, 1:1) to obtain the pure product as white powder. Yield: 2.15 g (68%). mp: 285 °C. <sup>1</sup>H NMR (400 MHz; CD<sub>2</sub>Cl<sub>2</sub>; Me<sub>4</sub>Si)  $\delta_H$  [ppm]: 1.48 (s, 9H), 7.11 (ddd,  $J = 24.5, 11.1, 4.8$  Hz, 8H), 7.29 (dt,  $J = 18.6, 8.3$  Hz, 6H), 7.47–7.59 (m, 7H), 7.64–7.82 (m, 6H), 8.76 (d,  $J = 8.1$  Hz, 1H), 8.79–8.86 (m, 2H).  $\delta_C$  (75 MHz; CD<sub>2</sub>Cl<sub>2</sub>; Me<sub>4</sub>Si)  $\delta_C$  31.34 (s), 35.14 (s), 121.17 (s), 122.67 (s), 123.38 (d), 123.76 (s), 124.18 (s), 124.87 (d), 125.65 (s), 126.48 (s), 127.10–127.86 (m), 128.35 (s), 128.71 (s), 128.73–129.61 (m), 129.76 (s), 133.96 (s), 136.31 (s), 137.52 (s), 140.75 (s), 147.80 (d,  $J = 3.9$  Hz), 150.81 (s), 153.72 (s). MS (ESI<sup>+</sup>):  $m/z$  670.6 (MH<sup>+</sup>). Calcd for C<sub>49</sub>H<sub>39</sub>N<sub>3</sub>: 669.31.

***N*-(4-(4-(2-(4-*tert*-Butylphenyl)-1*H*-phenanthro[9,10-*d*]imidazol-1-yl)phenyl)phenyl)-*N*-phenylbenzenamine (PATPA).** Using a similar approach for TPA-BPI by Suzuki coupling reaction, white powder was finally obtained. Yield: 2.54 g (76%). mp: 306 °C. <sup>1</sup>H NMR (300 MHz; CD<sub>2</sub>Cl<sub>2</sub>; Me<sub>4</sub>Si)  $\delta_H$  [ppm]: 1.31 (s, 9H), 7.06–7.23 (m, 7H), 7.29–7.39 (m, 8H), 7.53 (ddd,  $J = 8.4, 5.8, 2.5$  Hz, 1H), 7.61 (dd,  $J = 8.5, 2.1$  Hz, 4H), 7.69 (dd,  $J = 8.7, 2.0$  Hz, 3H), 7.72–7.80 (m, 2H), 7.87 (d,  $J = 8.6$  Hz, 2H), 8.72–8.82 (m, 3H).  $\delta_C$  (75 MHz; CD<sub>2</sub>Cl<sub>2</sub>) 31.10 (s), 121.11 (d), 122.70 (d), 123.48 (dd), 124.00–124.62 (m), 124.78–125.71 (m), 126.16 (d), 126.64 (s), 127.48 (d), 128.22 (dd), 129.04–129.43 (m), 129.60 (d), 130.23 (d), 130.84 (s), 131.66 (d), 132.44 (s), 133.10 (s), 137.56 (d), 139.04 (s), 141.12 (s), 142.05 (s), 147.71 (s), 148.39 (d), 151.13 (s), 152.26 (s). TOF-MS (EI<sup>+</sup>): Found: 669.27 (M<sup>+</sup>). Calcd for C<sub>49</sub>H<sub>39</sub>N<sub>3</sub>: 669.31.

***N*-(4-(5-(1-(4-*tert*-Butylphenyl)-1*H*-phenanthro[9,10-*d*]imidazol-2-yl)thiophen-2-yl)phenyl)-*N*-phenylbenzenamine (TPA-TPI).** TPA-TPI was synthesized using an approach similar to that in our previous work.<sup>27</sup> Yield: 2.3 g (99%). mp: 276 °C. <sup>1</sup>H NMR (400 MHz; CD<sub>2</sub>Cl<sub>2</sub>; Me<sub>4</sub>Si)  $\delta_H$  [ppm]: 1.53 (s, 9H), 6.64 (d,  $J = 4.0$  Hz, 1H), 7.02–7.17 (m, 9H), 7.23 (d,  $J = 7.3$  Hz, 1H), 7.27–7.37 (m, 5H), 7.42–7.65 (m, 5H), 7.69 (dd,  $J = 11.1, 4.2$  Hz, 1H), 7.77 (t,  $J = 7.4$  Hz, 3H), 8.61–8.93 (m, 3H);  $\delta_C$  (50 MHz; CDCl<sub>3</sub>; Me<sub>4</sub>Si) 31.52 (s), 35.19 (s), 120.64 (s), 122.51 (s), 123.17 (dd), 124.08 (s), 124.74 (d), 125.60 (s), 126.41 (d), 127.09 (d), 127.80 (d), 127.50 (s), 128.29 (d), 128.70 (s), 129.15 (s), 129.38 (s), 131.41 (s), 135.68 (s), 137.59 (s), 145.78 (s), 146.12 (s), 147.40 (s), 147.61 (s), 154.15 (s). MS (ESI<sup>+</sup>):  $m/z$  676.6 (MH<sup>+</sup>). Calcd for C<sub>47</sub>H<sub>37</sub>N<sub>3</sub>S: 675.27.

## RESULTS AND DISCUSSION

**X-ray Crystal Structures.** For the molecule structure determination, single crystals of TPA-BPI and BPA-BPI were grown by layering of *n*-hexane onto a dichloromethane solution of the compounds. Molecule structures of BPA-BPI and TPA-BPI (CCDC numbers are 840393 and 840394, respectively) are depicted in Figure 1. The benzene ring/*t*-Bu-benzene ring was highly twisted about the phenanthroimidazole plane with dihedral angles of 73° and 82° for BPA-BPI and TPA-BPI, respectively. These are expected to help suppress fluorescence quenching caused by aggregation in the solid state. The BPA moiety in BPA-BPI and the TPA moiety in TPA-BPI also

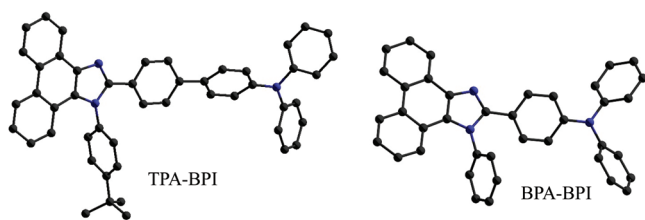


Figure 1. Molecule structures of TPA-BPI and BPA-BPI.

twisted about the phenanthroimidazole plane with dihedral angles of  $29^\circ$  and  $43^\circ$ , respectively. These would reduce the extent of conjugation in the molecules and thus the amount of charge transfer from the donor (i.e., BPA or TPA) to the acceptor (phenanthroimidazole).<sup>27</sup> The nonplanarity and the reduced extent of conjugation are beneficial for maintaining the short wavelength emission in solid state.<sup>28</sup>

**Thermal Properties.** The thermal properties of the four compounds were investigated with TGA and DSC under a nitrogen atmosphere, and their thermal data are summarized in Table 1. With the introduction of the rigid phenanthrobackbone and the TPA moiety, all compounds exhibit good thermal stability and film-forming ability. As shown in Figure 2, decomposition temperatures ( $T_d$ ), defined as the temperature at which the materials show a 5% weight loss, were measured to be 420, 375, 423, and 440  $^\circ\text{C}$  for TPA-BPI, BPA-BPI, PATPA, and TPA-TPI, respectively. Figure 3 shows DSC curves of the materials. Melting temperatures ( $T_m$ ) of the materials were observed upon heating up to 272–306  $^\circ\text{C}$ . The glass-transition temperatures ( $T_g$ ) of BPA-BPI, PATPA, and TPA-TPI were found to be 124, 141, and 121  $^\circ\text{C}$ , respectively. It is worth noting that, for TPA-BPI, no obvious  $T_g$  could be detected, and upon second heating, a crystallization temperature ( $T_c$ ) of 201  $^\circ\text{C}$  was observed.

**Optical Properties.** Photophysical properties of the four compounds were investigated by measuring the PL spectra in both dichloromethane solutions and solid-state thin films on quartz substrates. Key photophysical data are summarized in Table 1. As can be seen in Figure 4, all compounds exhibit broad structureless emission peaks ranging from 418 to 487 nm. The short emission wavelengths are attributed to the limited donor/acceptor charge transfer due to the nonplanarity and small extent of conjugation in the molecules.<sup>28</sup> It should be noted that all compounds show negligibly small peak shifts in their absorption and PL spectra from dichloromethane solutions to solid states. This indicates that the highly twisted substituent on the 1-imidazole position as well as the noncoplanar TPA moiety can effectively suppress the intermolecular  $\pi$ - $\pi$  stacking in the solid state. For the absorption spectra, it can be seen that all compounds show similar absorption bands at a wavelength of approximately 260 nm, which can be attributed to the  $\pi$ - $\pi^*$  transition of their

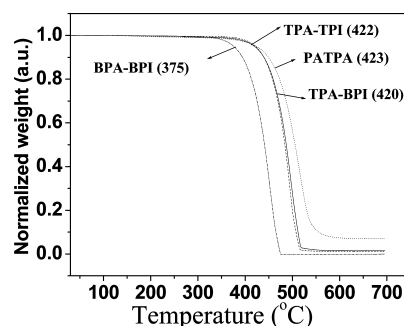


Figure 2. TGA curves for TPA-BPI, BPA-BPI, PATPA, and TPA-TPI.

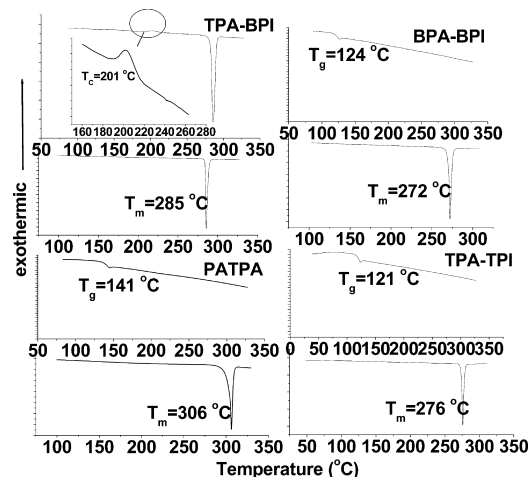


Figure 3. DSC curves for TPA-BPI, BPA-BPI, PATPA, and TPA-TPI.

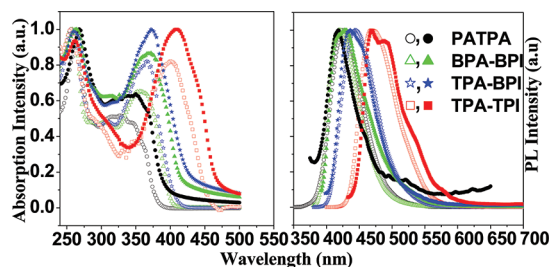


Figure 4. UV absorption and PL spectra of TPA-BPI, BPA-BPI, PATPA, and TPA-TPI in  $\text{CH}_2\text{Cl}_2$  solution (empty) and solid-state thin film (filled).

common thiophene ring and benzene ring.<sup>29</sup> The longer wavelength absorption bands vary in the range of 332–372 nm, which might be originated from the  $\pi$ - $\pi^*$  transition from the substituent on the 2-imidazole position to the phenanthroimidazole acceptor. On the other hand, it is worth noting that the PL spectrum of TPA-TPI is more red-shifted compared with those of other three compounds. It may be attributed to the

Table 1. Key Physical Properties of the Four Compounds

Compounds	$T_m/T_g/T_d$ ( $^\circ\text{C}$ )	solutionAbs (nm)	solutionPL (nm)	$\Phi_f^b$	filmAbs (nm)	filmPL (nm)	HOMO (eV) [optical/calculated]	LUMO (eV) [optical/calculated]	energy gap (eV) [optical/calculated]
TPA-BPI	285/201 <sup>a</sup> /420	256/361	442	~1	260/372	436	-5.26/-4.86	-2.36/-1.2	2.9/3.66
BPA-BPI	272/124/375	257/356	419	~1	263/369	428	-5.31/-4.78	-2.35/-0.99	2.96/3.79
PATPA	306/141/423	265/332	426		268/351	418	-5.54/-5.08	-2.39/-1.2	3.15/3.88
TPA-TPI	276/121/440	256/400	468	0.65	262/409	469/487	-5.00/-4.71	-2.41/-1.42	2.59/3.29

<sup>a</sup>Crystallization temperature. <sup>b</sup>Fluorescent quantum yield in solution measured with respect to anthracene.

lone pair electron on the thiophene group that requires a lower energy for the  $n-\pi^*$  transition.<sup>9,29</sup> In addition, the PL spectrum of TPA-BPI shows obvious solvatochromic shift, in which its emission color is red-shifted with increasing solvent polarity (Figure 5). This indicates the occurrence of charge transfer upon photoexcitation.<sup>30</sup>

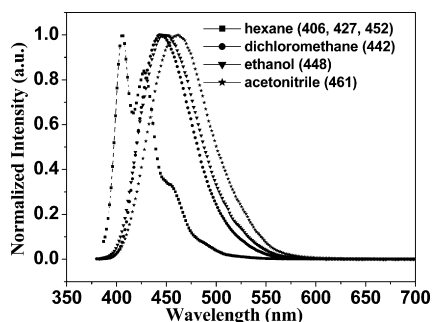


Figure 5. PL spectra of TPA-BPI dissolved in different solvents.

**Theoretical Calculation.** To gain insight into the electronic structures of the compounds, a DFT calculation was performed at the B3LYP/6-31G (d) level. As is shown in Figure 6, the HOMO levels mainly populate on the phenanthroimidazole moiety for all compounds and on the TPA moiety on all compounds except for PATPA. In other words, compared with the other three compounds, the TPA

moiety contributes less to the HOMO energy in PATPA. In fact, the HOMO level of PATPA was measured by UPS to be 5.54 eV, which is much larger than those of the other three compounds ranging from 5.00 to 5.31 eV. These results also suggest that the modification at the 1-position imidazole does not have significant effect on the HOMO energy of the compounds. The LUMO levels mostly populate on the imidazole ring and the linker between the donor and the acceptor. It is noted that the LUMO and HOMO both locate on the imidazole ring; on one hand it would contribute for the balanced charge transfer as the emitter in OLED, but on the other hand it could facilitate the charge transfer process upon excitation, which was also confirmed by the solvatochromic phenomenon observed in the solvent with a different polarity.

**Electroluminescent (EL) Properties.** EL properties of the four compounds were studied by using them as the emitters in trilayer OLEDs (anode/HTL/one of the four compounds as emitter/ETL/cathode) or the hole-transporting emitter in bilayer OLEDs (anode/one of the four compounds/ETL/cathode). Using the four materials, a total of 15 devices were fabricated. In these devices, ITO is used as the anode; NPB is used as the hole-transporting layer (HTL); TPBI, BPhen, or Alq<sub>3</sub> are used as the electron-transporting layer (ETL); and LiF/Al or LiF/Mg:Ag are used as the cathode. Detailed structures and key performance parameters of the 15 OLEDs and a reference NPB/Alq<sub>3</sub> device are summarized in Table 2.

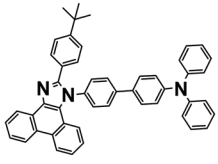
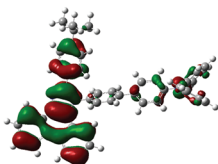
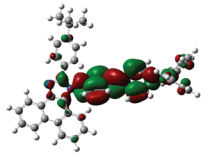
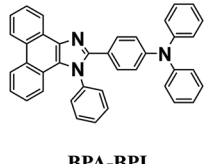
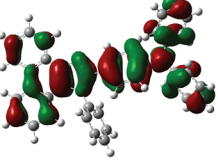
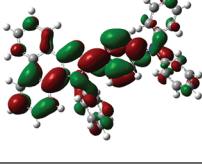
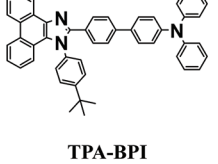
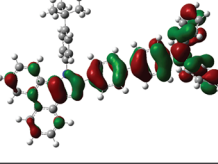
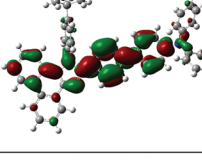
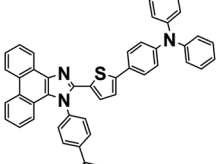
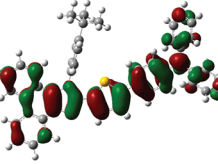
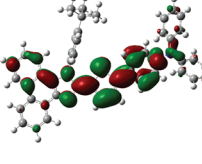
Compounds	HOMO	LUMO
 PATPA		
 BPA-BPI		
 TPA-BPI		
 TPA-TPI		

Figure 6. Spatial distributions of frontier orbitals of the PATPA, BPA-BPI, TPA-BPI, and TPA-TPI.

Table 2. Key Performance Parameters of Devices 1–16

	material						
	TPA-BPI		BPA-BPI		PATPA	TPA-TPI	
device	1/2	3/4	5/6/7	8/9	10/11/12	13	14/15/16
$V_{on}$ (V)	2.8/3.2	2.8/2.8	2.8/2.8/3.5	3.7/3.6	2/2.3/3.5	3.8	2.6/2.6/2.6
$\lambda_{maxEL}$	448/448	448/448	448/452/452	528/520	428/416/436	424	496/496/496
fwhm (nm)	71/71	71/71	73/69/75	98/96	65/57/53	63	80/80/42
CIE	(0.15, 0.09)	(0.15, 0.09)	(0.15, 0.09)	(0.32, 0.56)	(0.15, 0.05)	(0.15, 0.06)	(0.19, 0.39)
	(0.15, 0.09)	(0.15, 0.09)	(0.15, 0.09)	(0.32, 0.56)	(0.15, 0.05)		(0.17, 0.38)
			(0.15, 0.09)		(0.15, 0.05)		(0.18, 0.40)
$\eta_c^{max}$ (cd/A)	2.63/2.03	2.13/1.46	1.83/1.1/0.49	4.1/3.9	0.65/0.45/0.40	0.34	4.6/1.82/3
$\eta_p^{max}$ (lm/W)	2.53/1.81	1.85/1.34	1.58/0.75/0.17	2.8/2.5	0.68/0.47/0.35	0.24	4.68/1.9/2.9
$L$ (cd/m <sup>2</sup> ) at 100 mA/cm <sup>2</sup>	2259/1894	2085/1456	1820/1043/419	4069/3807	568/384/353	282	3222/1517/2465
$V^a$ (V)	4.6/5.3	5.6/4	4.7/4.4/8.6	7.2/5.7	3.6/3.9/7.1	5.3	4.4/4.1/4.2
$\eta_c^a$ (cd/A)	2.5 (2.42)/ 1.97 (1.90)	2.1 (2.10)/ 1.45 (1.46)	1.8/0.97/0.29	3.9/3.3	0.63/0.43/0.38	0.34	4/1.72/2.8
$\eta_p^a$ (lm/W)	1.7 (1.46)/1.1 (0.97)	1.2 (1.00)/1.1 (0.93)	1.2/0.67/0.16	1.7/1.8	0.55/0.34/0.16	0.2	2.8/1.32/2
EQE <sub>max</sub> (%)	3.08 (2.88)/ 2.34 (2.21)	2.62 (2.55)/ 1.77 (1.76)	2.14/1.19/0.51	1.30/1.23	1.37/0.66/0.85	0.72	1.91/0.75/1.24
TPA-BPI							
trilayer devices							
	1	ITO/NPB (60 nm)/TPA-BPI (40 nm)/TPBI (20 nm)/LiF (0.5 nm)/Al (80 nm)					
	2	ITO/NPB (60 nm)/TPA-BPI (40 nm)/Bphen (20 nm)/LiF (0.5 nm)/Al (80 nm)					
	3	ITO/NPB (60 nm)/TPA-BPI (40 nm)/TPBI (20 nm)/LiF (0.5 nm)/Mg:Ag (100 nm)					
	4	ITO/NPB (60 nm)/TPA-BPI (40 nm)/Bphen (20 nm)/LiF (0.5 nm)/Mg:Ag (100 nm)					
bilayer devices:							
	5	ITO/TPA-BPI (100 nm)/TPBI (20 nm)/LiF (0.5 nm)/Mg:Ag (100 nm)					
	6	ITO/TPA-BPI (100 nm)/Bphen (20 nm)/LiF (0.5 nm)/Mg:Ag (100 nm)					
single layer device:							
	7	ITO/TPA-BPI (120 nm)/LiF (0.5 nm)/Mg:Ag (100 nm)					
devices with Alq <sub>3</sub> :							
	8	ITO/TPA-BPI (70 nm)/Alq <sub>3</sub> (60 nm)/LiF (0.5 nm)/Mg:Ag (100 nm)					
	9	ITO/NPB (70 nm)/Alq <sub>3</sub> (60 nm)/LiF (0.5 nm)/Mg:Ag (100 nm)					
BPA-BPI							
	10	ITO/NPB (60 nm)/BPA-BPI (40 nm)/TPBI (20 nm)/LiF (0.5 nm)/Mg:Ag (100 nm)					
	11	ITO/NPB (60 nm)/BPA-BPI (40 nm)/Bphen (20 nm)/LiF (0.5 nm)/Mg:Ag (100 nm)					
	12	ITO/ITO/BPA-BPI (100 nm)/Bphen (20 nm)/LiF (0.5 nm)/Mg:Ag (100 nm)					
PATPA							
	13	ITO/NPB (60 nm)/PATPA (40 nm)/TPBI (20 nm)/LiF (0.5 nm)/Mg:Ag (100 nm)					
TPA-TPI							
	14	ITO/NPB (70 nm)/TPA-TPI (40 nm)/Bphen (20 nm)/LiF (0.5 nm)/Al (80 nm)					
	15	ITO/NPB (70 nm)/TPA-TPI (40 nm)/TPBI (20 nm)/LiF (0.5 nm)/Mg:Ag (100 nm)					
	16	ITO/TPA-TPI (110 nm)/TPBI (20 nm)/LiF (0.5 nm)/Mg:Ag (100 nm)					

<sup>a</sup>The former data was obtained at 20 mA/cm<sup>2</sup>; the data in brackets was obtained at high brightness of 1000 cd/m<sup>2</sup>.

Among the trilayer devices (devices 1–4, 10–16), device 1 based on TPA-BPI gives the best performance in terms of current, power efficiencies, and external quantum efficiency (EQE). In particular, maximum current, power, and external quantum efficiencies ( $\eta_c$ ,  $\eta_p$ , EQE) of respectively 2.63 cd/A, 2.53 lm/W, and 3.08% were obtained. The device also has a low onset voltage (defined as the voltage required to obtain a luminance of 1 cd/m<sup>2</sup>) of 2.8 V and low operating voltages (5.19 and 4.6 V, respectively, to give a current density of 20 mA/cm<sup>2</sup> and a luminance of 1000 cd/m<sup>2</sup>). All the TPA-BPI-based trilayer devices (devices 1–4) exhibit steady saturated blue emission of CIE coordinates (0.15, 0.09) (peaked at 448 nm) over a wide range of operation conditions (Figures 7 and 8).

By comparing to the performance of the bilayer (devices 5–6) devices using TPA-BPI as both the HTL and the emitter, it can be seen (Table 1 and Figure 9) that TPA-BPI has good hole-transporting properties. In fact, the current densities of the bilayer devices (5 and 6) are slightly higher than those of the corresponding trilayer devices (3 and 4). For instance, at a driving voltage of 5 V, the current density of device 5 is 31

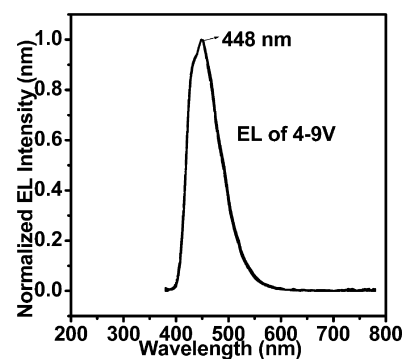


Figure 7. EL spectra for trilayer device 1 at different voltages from 4–9 V.

mA/cm<sup>2</sup>, while that of device 3 is 13 mA/cm<sup>2</sup>. This may be attributed to the shallow HOMO levels of TPA-BPI (5.26 eV) comparing to that of NPB (5.40 eV). Device 5 also shows a reasonably high efficiency ( $\eta_c = 1.83$  cd/A;  $\eta_p = 1.58$  lm/W; EQE = 2.14%), low onset voltage of 2.8 V, and low operation

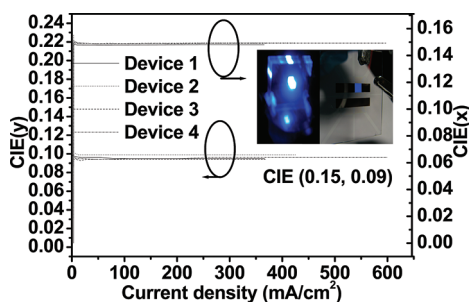


Figure 8.  $CIE_x$  and  $CIE_y$  at different current densities up to 600  $\text{mA}/\text{cm}^2$  for the TPA-BPI based devices 1–4.

voltage (20  $\text{mA}/\text{cm}^2$  at 4.7 V, 5.7 V for 1000  $\text{cd}/\text{m}^2$ ), suggesting that TPA-BPI is also a promising hole-transporting material. To further confirm the hole-transporting properties of TPA-BPI, a bilayer device (TPA-BPI/Alq<sub>3</sub>, device 8) was made and compared with the standard NPB/Alq<sub>3</sub> device (device 9). Device 8 shows higher maximum efficiencies (4.1  $\text{cd}/\text{A}$ , 2.8  $\text{lm}/\text{W}$ , 1.3%) than those of device 9 (3.9  $\text{cd}/\text{A}$ , 2.5  $\text{lm}/\text{W}$ , 1.23%), confirming that the TPA-BPI is also a promising hole-transporting material.

To explore the possible bipolar transporting properties of TPA-BPI, a single layer device (device 7) with a structure of ITO/TPA-BPI/LiF/Mg:Ag was also fabricated. However, it was found that the maximum device efficiencies (i.e., 0.49  $\text{cd}/\text{A}$ , 0.17  $\text{lm}/\text{W}$ , 0.51%) are far below those of the bilayer devices (devices 5 and 6). The poor performance may be due to a large electron-injection barrier at the TPA-BPI/LiF interface ( $\sim 0.54$  eV). On the other hand, it is worth noting that all the TPA-BPI based devices show little efficiency roll-off as current density increases (Figure 10). Together with their stable emission color, TPA-BPI is suitable for applications requiring high brightness deep-blue emission.

To further access the performance of TPA-BPI as a deep-blue emitter, performance of device 1 (trilayer) and device 5 (bilayer) are compared with those of similarly structured deep-blue emitting devices reported recently (Table 3).<sup>6–19,31–37</sup> It can be seen that the performance of the TPA-BPI based devices are among the best in terms of turn-on/operation voltages and efficiency for nondoped devices with  $CIE_y < 0.10$ .<sup>6–19,31–37</sup>

Comparing to TPA-BPI, devices using BPA-BPI or PATPA as emitters show even more saturated blue emissions. Particularly, the BPA-BPI based device showed a violet-blue emission with CIE coordinates of (0.15, 0.05) and a relatively

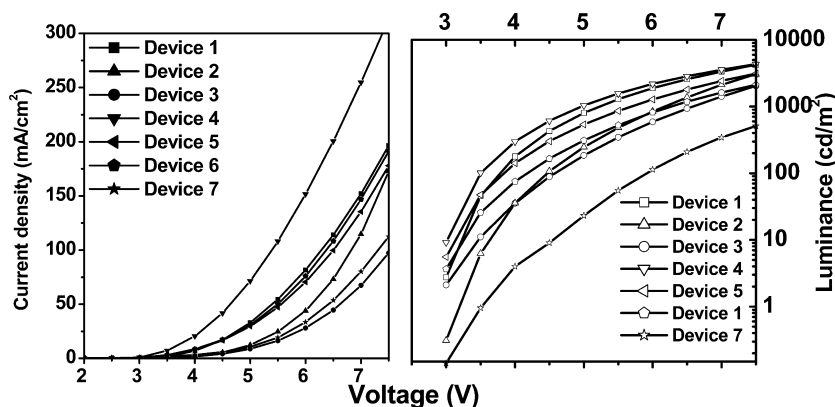


Figure 9. Current density ( $J$ - $V$ ) and luminance ( $L$ - $V$ ) at different driving voltages for the TPA-BPI based devices 1–7.

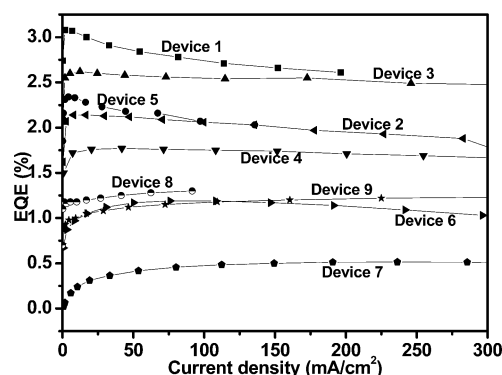


Figure 10. EQE at different current densities for the TPA-BPI based devices 1–9.

narrow full width at half-maximum (fwhm) of 65, 57, and 53 nm for trilayer devices 10 and 11 and bilayer device 12, respectively. For PATPA, the maximum EL peak further blue-shifted to 424 nm with a fwhm of 63 nm (device 13). This blue shift on the EL spectra may be due to shorter conjugation lengths of BPA-BPI and PATPA compared to that of TPA-BPI. As aforementioned, the highly twisted TPA moiety can intervene with the conjugation to reduce the extent of charge transfer from the donor (i.e., BPA) to the acceptor (phenanthroimidazole), leading to a blue-shifted EL. On the other hand, performances of the BPA-BPI and PATPA based devices are not as good as those of the TPA-BPI based devices. For example, maximum EQE of the trilayer devices based on BPA-BPI, PATPA, and TPA-BPI (devices 10, 13, and 1) are 1.37, 0.72, and 3.08%, respectively.

The fourth compound TPA-TPI possesses a higher-lying HOMO energy of 5.00 eV, which is much smaller than those of other three compounds (5.26, 5.31, and 5.54 eV). It also has a smaller energy gap of 2.59 eV compared to the values of about 3 eV for the other three compounds. As expected, the device (device 14) based on TPA-TPI shows higher efficiencies (4.6  $\text{cd}/\text{A}$  and 4.68  $\text{lm}/\text{W}$ ), while the blue emission is less saturated (peaked at 496 nm, with CIE coordinates of (0.19, 0.39)). It was found that TPA-TPI can also act as a hole-transporting material. In particular, bilayer device 16 (TPA-TPI/TPBI) shows a better performance in terms of current, power efficiencies, and EQE (Table 2) than those of trilayer device 15 (NPB/TPA-TPI/TPBI). As shown in Figure 11, at the same driving voltage, the current density of the bilayer device 16 is only slightly lower than that of the trilayer device 15, which

Table 3. Key Characteristics of Devices 1 and 5 and Other Recently Reported Non-Doped Blue Emitting Devices with CIE<sub>y</sub> < 0.1

emitter	HOMO	V <sub>on</sub> <sup>a</sup> (V)	EL (nm)	η <sub>c</sub> <sup>maxb</sup> (cd/A)	η <sub>p</sub> <sup>b</sup> (lm/W)	CIE 1931 (x, y)	ref
TPA-BPI	5.26	2.8	448	2.63/2.5 <sup>c</sup> /2.6 <sup>h</sup>	2.53/1.7 <sup>c</sup> /2.0 <sup>h</sup>	(0.15, 0.09)	this work
TPA-BPI <sup>d</sup>	5.26	2.8	448	1.83/1.8 <sup>c</sup>	1.58/1.2 <sup>c</sup>	(0.15, 0.09)	this work
DMIP-2-NA	5.55	5.77	460	1.17	0.64	(0.151, 0.097)	6
CzPhB	5.92	6.5	449	3.3	1.3	(0.15, 0.09)	7
OPVs1	6.08	4.5	452	1.29 <sup>c</sup>	0.66 <sup>c</sup>	(0.14, 0.08)	8
DNBN	6.0	–	444	1.84	1.13	(0.15, 0.08)	9
NATSNA <sup>f</sup>	5.9	–	438	2	–	(0.16, 0.097)	10
4a	5.8	4.1	444	1.9/1.16 <sup>c</sup>	1.56/0.49 <sup>c</sup>	(0.154, 0.08)	11
5a	5.89	3.0	444	2.8/1.67 <sup>c</sup>	2.33/1.05 <sup>c</sup>	(0.153, 0.079)	11
MADN	–	4	442	1.35/1.08 <sup>c</sup>	1.01/0.48 <sup>c</sup>	(0.153, 0.08)	11
TP-EPY	6.03	9.2	453	1.72	0.65	(0.154, 0.068)	12
TP-EIF	5.94	11.2	430	0.76	0.27	(0.163, 0.073)	12
TBMFA <sup>g</sup>	5.79	3.2	444	1.79	1.41	(0.151, 0.085)	13
TBDNPA <sup>g</sup>	5.83	3.0	444	2.63	1.96	(0.149, 0.086)	13
TBMFPA <sup>g</sup>	5.82	3.2	448	2.67	1.92	(0.147, 0.096)	13
In2Bt	5.7	3	439	0.86	0.76	(0.16, 0.08)	14
ADF	5.73	9.5 <sup>c</sup>	460	0.85	–	(0.15, 0.08)	15
sFTaz	5.6	8.1	428	0.8	–	(0.17, 0.08)	16
α,α-MADN	5.8	6.7	–	0.7	0.3	(0.15, 0.08)	17
CPhBzIm	5.49	–	–	1.6	1.07	(0.16, 0.05)	17
Cz-NPh	5.12	3	456	1.96	1.51	(0.14, 0.09)	18
TPIP <sup>i</sup>	5.4	3.9	445	4.69/4.67 <sup>h</sup>	2.71/2.14 <sup>h</sup>	(0.15, 0.09)	19
BH-1SN	–	–	–	0.61 <sup>c</sup>	1.37	(0.15, 0.08)	31
DSX-IF	–	–	414	1	0.3	(0.19, 0.08)	32
TFSTPA	5.32	–	–	1.63	–	(0.16, 0.07)	33
o,p-TP-EPY	–	–	440	1.17	0.3	(0.156, 0.078)	34
T3	5.38	5	414	0.47	–	(0.16, 0.07)	35
PhQ-CVz <sup>e</sup>	–	~3.5	–	2.06/1.90 <sup>c</sup>	1.77/0.85 <sup>c</sup>	(0.156, 0.093)	36
POAn	2.5	–	445	3.2	3.3	(0.15, 0.07)	37

<sup>a</sup>V<sub>on</sub> is onset voltage obtained at 1 cd/m<sup>2</sup>. <sup>b</sup>η<sub>c</sub><sup>max</sup> and η<sub>p</sub><sup>max</sup> are maximum current efficiency and power efficiency, respectively. <sup>c</sup>Obtained at 20 mA/cm<sup>2</sup>. <sup>d</sup>Bilayer device. <sup>e</sup>2NATA inserted. <sup>f</sup>m-MTDATA inserted. <sup>g</sup>PEDOT:PSS inserted. <sup>h</sup>Obtained at 200 cd/m<sup>2</sup>. <sup>i</sup>BCP and Alq<sub>3</sub> were matched as electron transport layer.

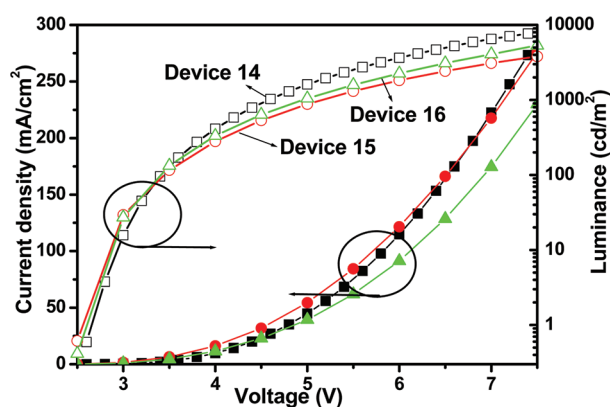


Figure 11. Current density ( $J$ - $V$ ) and luminance ( $L$ - $V$ ) at different driving voltages for the TPA-TPI based devices 14–16.

uses NPB as the HTL, while the brightness of bilayer device 16 is higher than that of trilayer device 15. Again, efficiencies of the TPA-TPI based devices only show mild decreases at high current densities (Figure 12). This suggests that TPA-TPI is also a promising candidate for a blue emitter.

By combining the advantages of the phenanthroimidazole backbone and the donor- $\pi$ -acceptor structure, a deep-blue emitter TPA-BPI with high fluorescence efficiency and appropriate HOMO/LUMO energy levels was obtained.

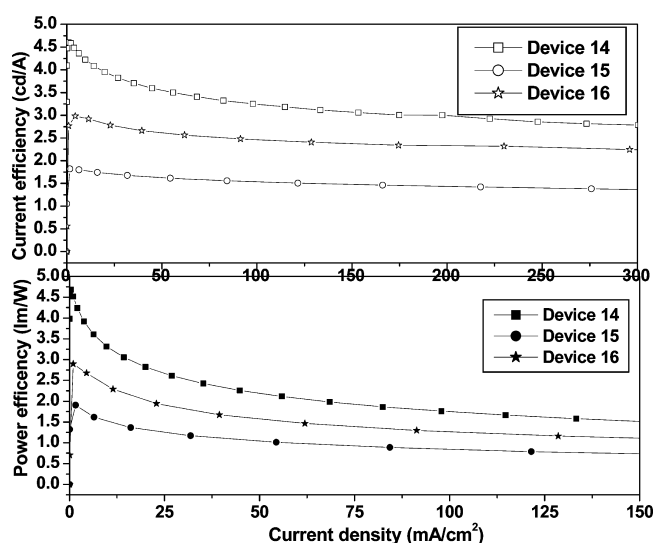


Figure 12. Power efficiency and current efficiency at different current densities for the TPA-TPI based devices 14–16.

Reservation of phenanthroimidazole's deep-blue emission was realized by limiting charge transfer and extension of conjugation via nonplanarity of the molecule. The linker between donor and acceptor moieties and the donor position on the skeleton were considered key factors for obtaining a



high efficiency deep-blue emitter in this system. Different linkers attaching on the 2-position imidazole as well as the disturbed conjugation could affect the extent of the charge transfer process in this system. Besides, the highly twisted moiety on the 1-position of the imidazole skeleton can prevent the aggregation in the solid state caused by molecule interaction. High performance deep-blue emitting devices were realized with the present materials serving as both the emitter and the HTL. It was foreseen that the device performance might be able to be further improved if the electron-transporting properties of the present materials could be enhanced to give a more balanced carrier transport. Thus, further work would be performed by changing the different linkers with different electron transport abilities between the donor and the acceptor on 2-position imidazole.

## CONCLUSION

In summary, we have designed and synthesized three phenanthroimidazole-based materials with a donor- $\pi$ -acceptor structure by attaching the strong electron-donating moiety of triphenylamine (TPA) to different positions of the phenanthroimidazole with different linkers and investigated their applications in nondoped OLEDs. The fluorophores show high quantum yields (up to  $\sim 1$ ) and good thermal stability. A TPA-BPI trilayer device exhibits high efficiencies of 2.63 cd/A, 2.53 lm/W, and 3.08%, low onset voltage of 2.8 V, and low operating voltage (i.e., 5.19 V for 20 mA/cm<sup>2</sup>, 4.6 V for 1000 cd/m<sup>2</sup>) as well as a deep-blue emission with CIE coordinates of (0.15, 0.09) and little efficiency roll-off and color change at high brightness. By reducing the extent of conjugation in BPA-BPI and PATPA, the EL spectra of their devices are further blue-shifted to show violet blue emission with CIE coordinates of (0.15, 0.05) and (0.15, 0.06), respectively. Together with their good hole-transporting properties, the four new materials are considered to have good potential for applications in blue OLEDs requiring operation at high excitation densities.

## ASSOCIATED CONTENT

### Supporting Information

Tables of crystal data, structure solution and refinement, atomic coordinates, bond lengths and angles, and anisotropic thermal parameters for TPA-BPI and BPA-BPI and UPS spectra for the reported materials (PDF). Two X-ray crystallographic file for TPA-BPI and BPA-BPI (CIF). This material is available free of charge via the Internet at <http://pubs.acs.org>.

## ACKNOWLEDGMENTS

This work was supported by the Research Grants Council of the Hong Kong Special Administrative Region, China (Project No. CityU 101508), National Natural Science Foundation of China (No. 91027041), and the Key Laboratory of Photochemical Conversion and Optoelectronic Materials, TIPC, CAS.

## REFERENCES

(1) (a) Tung, Y. J.; Ngo, T.; Hack, M.; Brown, J.; Koide, N.; Nagara, Y.; Kato, Y.; Ito, H. *Dig. Tech. Pap. - Soc. Inf. Disp. Int. Symp.* **2004**, *35*, 48. (b) Wen, S. W.; Lee, M. T.; Chen, C. H. *J. Disp. Technol.* **2005**, *1*, 90. (c) Gao, Z. Q.; Mi, B. X.; Chen, C. H.; Cheah, K. W.; Cheng, Y. K.; Wen, W. S. *Appl. Phys. Lett.* **2007**, *90*, 123506. (d) Su, S. J.; Cai, C.; Kido, J. *J. Chem. Mater.* **2011**, *23*, 274.

(2) Holmes, R. J.; Forrest, S. R.; Sajoto, T.; Tamayo, A.; Djurovich, P. I.; Thompson, M. E.; Brooks, J.; Tung, Y. J.; D'Andrade, B. W.;

Weaver, M. S.; Kwong, R. C.; Brown, J. *J. Appl. Phys. Lett.* **2005**, *87*, 243507.

(3) (a) Matsumoto, N.; Miyazaki, T.; Nishiyama, M.; Adachi, C. *J. Phys. Chem. C* **2009**, *113*, 6261. (b) Yang, Y. X.; Cohn, P.; Dyer, A. L.; Eom, S. H.; Reynolds, J. R.; Castellano, R. K.; Xue, J. G. *Chem. Mater.* **2010**, *22*, 3580.

(4) Baldo, M. A.; O'Brien, D. F.; You, Y.; Shoustikov, A.; Sibley, S.; Thompson, M. E.; Forrest, S. R. *Nature* **1998**, *395*, 151.

(5) (a) Gu, J. F.; Xie, G. H.; Zhang, L.; Chen, S. F.; Lin, Z. Q.; Zhang, Z. S.; Zhao, J. F.; Xie, L. H.; Tang, C.; Zhao, Y.; Liu, S. Y.; Huang, W. J. *Phys. Chem. Lett.* **2010**, *1*, 2849. (b) Tao, S.; Zhou, Y.; Lee, C. S.; Lee, S. T.; Huang, D.; Zhang, X. H. *J. Phys. Chem. C* **2008**, *112*, 14603. (c) Tong, Q. X.; Lai, S. L.; Chan, M. Y.; Zhou, Y. C.; Kwong, H. L.; Lee, C. S.; Lee, S. T. *Chem. Mater.* **2008**, *20*, 6310.

(6) Xia, Z. Y.; Zhang, Z. Y.; Su, J. H.; Zhang, Q.; Fung, K. M.; Lam, M. K.; Li, K. F.; Wong, W. Y.; Cheah, K. W.; Tian, H.; Chen, C. H. *J. Mater. Chem.* **2010**, *20*, 3768.

(7) Lin, S. L.; Chan, L. H.; Lee, R. H.; Yen, M. Y.; Kuo, W. J.; Chen, C. T.; Jeng, R. J. *Adv. Mater.* **2008**, *20*, 3947.

(8) Moorthy, J. N.; Venkatakrishnan, P.; Natarajan, P.; Lin, Z. H.; Chow, T. J. *J. Org. Chem.* **2010**, *75*, 2599.

(9) Seo, J. H.; Lee, K. H.; Seo, B. M.; Koo, J. R.; Moon, S. J.; Park, J. K.; Yoon, S. S.; Kim, Y. K. *Org. Electron.* **2010**, *11*, 1605.

(10) Lyu, Y. Y.; Kwak, J. H.; Kwon, O.; Lee, S. H.; Kim, D.; Lee, C. H.; Char, K. *Adv. Mater.* **2008**, *20*, 2720.

(11) Park, J. K.; Lee, K. H.; Kang, S.; Lee, J. Y.; Park, J. S.; Seo, J. H.; Kim, Y. K.; Yoon, S. S. *Org. Electron.* **2010**, *11*, 905.

(12) Park, Y.; Lee, J. H.; Jung, D. H.; Liu, S. H.; Lin, Y. H.; Chen, L. Y.; Wud, C. C.; Park, J. *J. Mater. Chem.* **2010**, *20*, 5930.

(13) Zheng, C. J.; Zhao, W. M.; Wang, Z. Q.; Huang, D.; Ye, J.; Ou, X. M.; Zhang, X. H.; Lee, C. S.; Lee, S. T. *J. Mater. Chem.* **2010**, *20*, 1560.

(14) Tsai, T. C.; Hung, W. Y.; Chi, L. C.; Wong, K. T.; Hsieh, C. C.; Chou, P. T. *Org. Electron.* **2009**, *10*, 158.

(15) Culligan, S. W.; Chen, A. C. A.; Wallace, J. U.; Klubek, K. P.; Tang, C. W.; Chen, S. H. *Adv. Funct. Mater.* **2006**, *16*, 1481.

(16) Lei, T.; Luo, J.; Wang, L.; Ma, Y. G.; Wang, J.; Cao, Y.; Pei, J. *New J. Chem.* **2010**, *34*, 699.

(17) Ho, M. H.; Wu, Y. S.; Wen, S. W.; Lee, M. T.; Chen, T. M.; Chen, C. H.; Kwok, K. C.; So, S. K.; Yeung, K. T.; Cheng, Y. K.; Gao, Z. Q. *Appl. Phys. Lett.* **2006**, *89*, 252903.

(18) Kuo, W. J.; Lin, S. L.; Chen, S. D.; Chang, C. P.; Lee, R. H.; Jeng, R. J. *Thin Solid Films.* **2008**, *516*, 4145.

(19) Kuo, C. J.; Li, T. Y.; Lien, C. C.; Liu, C. H.; Wub, F. I.; Huang, M. J. *J. Mater. Chem.* **2009**, *19*, 1865.

(20) Gong, S. L.; Zhao, Y. B.; Wang, M.; Yang, C. L.; Zhong, C.; Qin, J. G.; Ma, D. G. *Chem. Asian J.* **2010**, *5*, 2093.

(21) Xiao, H. B.; Shen, H.; Lin, Y. G.; Su, J. H.; Tian, H. *Dyes Pigm.* **2007**, *73*, 224.

(22) Chen, C. H.; Huang, W. S.; Lai, M. Y.; Tsao, W. C.; Lin, J. T.; Wu, Y. H.; Ke, T. H.; Chen, L. Y.; Wu, C. C. *Adv. Funct. Mater.* **2009**, *19*, 2661.

(23) Hudson, Z. M.; Wang, S. *Acc. Chem. Res.* **2009**, *42*, 1584.

(24) Mahesh, V. K.; Maheswari, M.; Sharma, R. *Can. J. Chem.* **1985**, *63*, 632.

(25) Miyaura, N.; Suzuki, A. *Chem. Rev.* **1995**, *95*, 2457.

(26) Eaton, D. F.; Houk, K. N.; Iwamura, H.; Kuzmin, M. G.; Michl, J.; Tokumaru, K. *Pure Appl. Chem.* **1988**, *60*, 1107.

(27) Zhang, Y.; Lai, S. L.; Tong, Q. X.; Chan, M. Y.; Ng, T. W.; Wen, Z. C.; Zhang, G. Q.; Lee, S. T.; Kwong, H. L.; Lee, C. S. *J. Mater. Chem.* **2011**, *21*, 8206.

(28) Huang, J. H.; Su, J. H.; Li, X.; Lam, M. K.; Fung, K. M.; Fan, H. H.; Cheah, K. W.; Chen, C. H.; Tian, H. *J. Mater. Chem.* **2011**, *21*, 2957.

(29) Yan, Y. N.; Pan, W. L.; Song, H. C. *Dyes Pigm.* **2010**, *86*, 249.

(30) Hung, W. Y.; Chi, L. C.; Chen, W. J.; Chen, Y. M.; Chou, S. H.; Wong, K. T. *J. Mater. Chem.* **2010**, *20*, 10113.

(31) Jeon, S. O.; Jeon, Y. M.; Kim, J. W.; Lee, C. W.; Gong, M. S. *Org. Electron.* **2008**, *9*, 522.

- (32) Cocherel, N.; Poriel, C.; Vignau, L.; Franc, J.; Bergamini, O.; Berthelot, J. R. *Org. Lett.* **2010**, *12*, 452.
- (33) Jiang, Z. Q.; Liu, Z. Y.; Yang, C. L.; Zhong, C.; Qin, J. G.; Yu, G.; Liu, Y. Q. *Adv. Funct. Mater.* **2009**, *19*, 3987.
- (34) Parka, Y.; Seoka, C. H.; Lee, J. H.; Parka, J. *Synth. Met.* **2010**, *160*, 845.
- (35) Liu, Q. D.; Lu, J. P.; Ding, J. F.; Day, M.; Tao, Y.; Barrios, P.; Stupak, J.; Chan, K.; Li, J. J.; Chi, Y. *Adv. Funct. Mater.* **2007**, *17*, 1028.
- (36) Lee, S. J.; Park, J. S.; Yoon, K. J.; Kim, Y. I.; Jin, S. H.; Kang, S. K.; Gal, Y. S.; Kang, S. W.; Lee, J. Y.; Kang, J. W.; Lee, S. H.; Park, H. D.; Kim, J. J. *Adv. Funct. Mater.* **2008**, *18*, 3922.
- (37) Chien, C. H.; Chen, C. K.; Hsu, F. M.; Shu, C. F.; Chou, P. T.; Lai, C. H. *Adv. Funct. Mater.* **2009**, *19*, 560.